

Langmuir probe measurements in the intense RF field of a helicon discharge

Francis F Chen

Electrical Engineering Department, University of California, Los Angeles, CA 90095-1994, USA

Received 21 May 2012, in final form 12 July 2012

Published 6 September 2012

Online at stacks.iop.org/PSST/21/055013

Abstract

Helicon discharges have extensively been studied for over 25 years both because of their intriguing physics and because of their utility in producing high plasma densities for industrial applications. Almost all measurements so far have been made away from the antenna region in the plasma ejected into a chamber where there may be a strong magnetic field (B -field) but where the radiofrequency (RF) field is much weaker than under the antenna. Inside the source region, the RF field distorts the current–voltage (I – V) characteristic of the probe unless it is specially designed with strong RF compensation. For this purpose, a thin probe was designed and used to show the effect of inadequate compensation on electron temperature (T_e) measurements. The subtraction of ion current from the I – V curve is essential; and, surprisingly, Langmuir's orbital motion limited theory for ion current can be used well beyond its intended regime.

(Some figures may appear in colour only in the online journal)

1. Introduction

It is well known that electrostatic probes in a plasma with sinusoidal oscillations in plasma (space) potential V_s will have distorted current–voltage (I – V) characteristics because what is measured is the dc average of a nonlinear I – V relationship [1–3]. This effect is shown in figure 1. A sinusoidal oscillation of peak amplitude 15 V in plasma potential V_s is assumed. The thick curve at the center is an ideal OML curve, and the side curves show the shifted I – V curves as seen by an uncompensated probe at various phases of the radiofrequency (RF). Since the curves are nonlinear, the current averaged over the oscillations will differ from the correct value. For instance, the dashed line shows the current at at probe voltage $V_p = 20$ V. The average over the shifted currents at that voltage would be lower than the unshifted current. What is worse, the shift stays longer at the extremes of the shift (± 15 V here) than at other phases as the voltage turns around. The yellow circles (color online) show the dc average current computed taking this effect into account. The result is that the slope of the I – V curve is decreased, leading to a spuriously high apparent KT_e . It is seen that the error becomes smaller as the probe approaches electron saturation, where the nonlinearity is less strong.

The ion part of figure 1 is shown in figure 2 by a change of scale. The RF-distorted curve is shown there by the yellow squares. It is seen that the ion saturation current, I_{sat} , where V_p

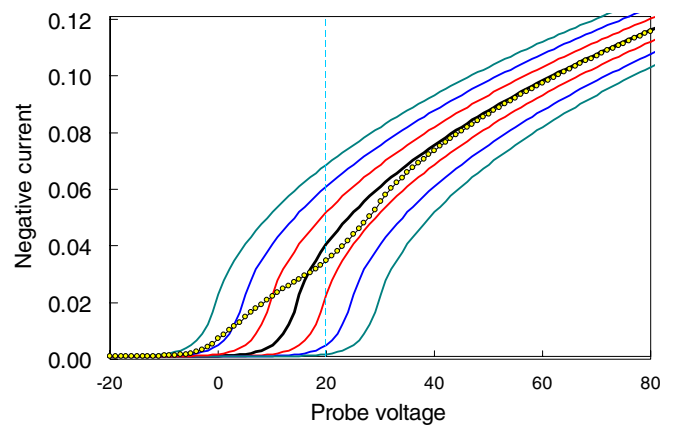


Figure 1. Effect of RF oscillations on electron probe currents to a Langmuir probe. The thick center curve is the theoretical orbital motion limited (OML) current (amperes) to a probe 0.15 mm in diameter and 10 mm long in an argon plasma of density 10^{11} cm $^{-3}$. The shifted I – V curves are for $V_s - V_p = \pm 5, \pm 10$ and ± 15 V. The circles show the dc current averaged over the oscillations.

is negative enough that negligible electron current is collected, follows the correct curve almost exactly. This is because I_{sat} varies very slowly with V_p .

In principle, a Maxwellian electron distribution with temperature T_e would give an exponentially rising I – V curve

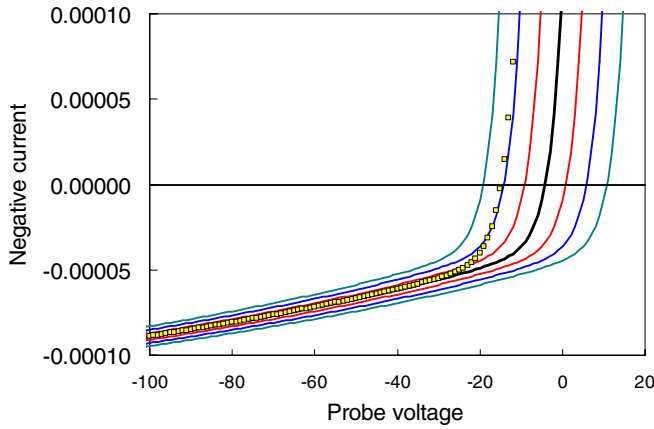


Figure 2. The ion part of figure 1 shown by changing the scales of the plot. The yellow squares (color online) show the time-averaged curve with no RF compensation.

up to V_s , at which point saturation occurs, and $|dI/dV|$ reaches a maximum. Normally, electron saturation current would be a square root of the mass ratio larger than ion saturation current, and the onset of electron saturation would be marked by a distinct ‘knee’ in the $I-V$ curve. However, collisions make the knee more rounded, and magnetic fields make the knee occur at much lower voltages. To obtain enough e-foldings in the exponential part of the $I-V$ curve and to obtain a value for T_e , it is then necessary to use the part of the $I-V$ curve that contains some ion current; namely, the part near the floating potential V_f , where $I = 0$. Since the ion current I_i has to be subtracted from I to obtain I_e , one must have a theory for I_i .

The behavior of I_{sat} has been calculated for collisionless plasmas by Mott-Smith and Langmuir [4], by Allen, Boyd and Reynolds [5] (ABR), and by Bernstein, Rabinowitz [6] and Laframboise [7] (BRL). These theories have been summarized [8] and parametrized [9] for easy use by Chen. The BRL and ABR theories have been found to be inaccurate for partially ionized industrial plasmas [10], while the Langmuir OML theory appears to be useful well beyond its intended range of applicability [11]. It is Langmuir’s simple formula for I_i , equation (1), that fits experiments well, not his more complete error-function formula, which was used to compute I_e in figure 1:

$$I_i = A_p n e \frac{\sqrt{2}}{\pi} \left(\frac{e V_p}{M} \right)^{1/2}, \quad I_i^2 \propto V_p. \quad (1)$$

Here A_p is the probe surface area, n is the plasma density, e is the unit charge and M is the ion mass. This formula does not depend on KT_e , so n can be determined by fitting a straight line to the slope of an I^2-V plot. Once n is known, and if the electrons are Maxwellian, KT_e and V_s can be determined from equation (2). Here v_{the} is the electron random thermal velocity. On a plot of $\ln(I_e)$ versus V_p , a straight-line fit’s slope will give KT_e , and the line’s horizontal position will yield V_s if n is known. This procedure will be clear when the data are presented:

$$I_e = n e v_{the} e^{(V_p - V_s)/KT_e}. \quad (2)$$

Some commercial probe systems use equation (1) to analyze ion current. For instance, this is carried out in the Hiden

Analytical’s ESPsoft® software [12], and in the SLP2000 system of Plasmart in Korea (no longer available). Other systems treat ion current differently. The Impedans [13] ALP system uses the BRL theory with a correction for collisions. The Korean Wise Probe [14] of Chin Wook Chung applies an ac signal to a floating probe and deduces plasma parameters from the harmonics without a direct measurement of I_{sat} . We have chosen to use the OML theory not only because of its simplicity but also because it has been calibrated against microwave interferometry, with result that it is accurate in the 10 mTorr range of pressures and is in error by at most a factor of 2 at 1 mTorr. The use of equations (1) and (2), in that order, yields n and KT_e without iteration between them. Some systems require finding V_s from the knee in the $I-V$ curve, but this method fails in the presence of magnetic fields and collisions.

2. Apparatus

2.1. Helicon discharge

The helicon discharge is shown in figure 3. The dc magnetic field is provided by an annular permanent magnet placed at an optimized height above the discharge tube. The use of the remote, reverse field of such a magnet has been described previously [15–17]. The quartz discharge tube has an inner diameter of 5.2 cm and a height of 5.8 cm. The entire superstructure was built only to accommodate the vertical probe; it is not necessary for the discharge. The loop antenna is placed at the bottom to eject the most plasma down into a large chamber. RF frequencies of 27.12 and 13.56 MHz have been used. The magnet height is adjusted to give the B -field for highest downstream density. At 27.12 MHz, this field varies from 80 G at the top to 39 G at the bottom, with an average of 60 G. The chamber above the discharge was made for the vertical probe that probes the discharge interior. It was not possible to make a port for a radial probe without destroying the azimuthal symmetry of this small tube. The top of the discharge is normally a solid, grounded aluminum plate placed so that the helicon wave reflected from it interferes constructively with the downward wave (the low field peak effect [18]). To insert the probe, the top plate is replaced with one that has a 1/8 inch (3.2 mm) diameter hole through which two alumina probe shafts are inserted, one for the probe and the other for the compensation electrode (CE). Other holes, arbitrarily placed, are for pumping the probe extension. Normal operation is at 400 W of RF at 27.12 MHz and 15 mTorr of argon, but power has been varied from 200 to 1000 W, and pressure from 10 to 60 mTorr. Data given here are for normal conditions unless otherwise specified.

2.2. The Langmuir probe

The probe shaft is a 1.6 mm diameter alumina tube 11 cm long suspended in a 1/4 inch (6.4 mm) tube with the vacuum seal at the upper end. The larger tube houses the inductors (chokes) for filtering out the RF pickup. The probe tip is a tungsten rod 5 mil (0.127 mm) in diameter and 7 mm long. It is spot-welded to a 10 mil diameter tungsten rod within the thin tube,

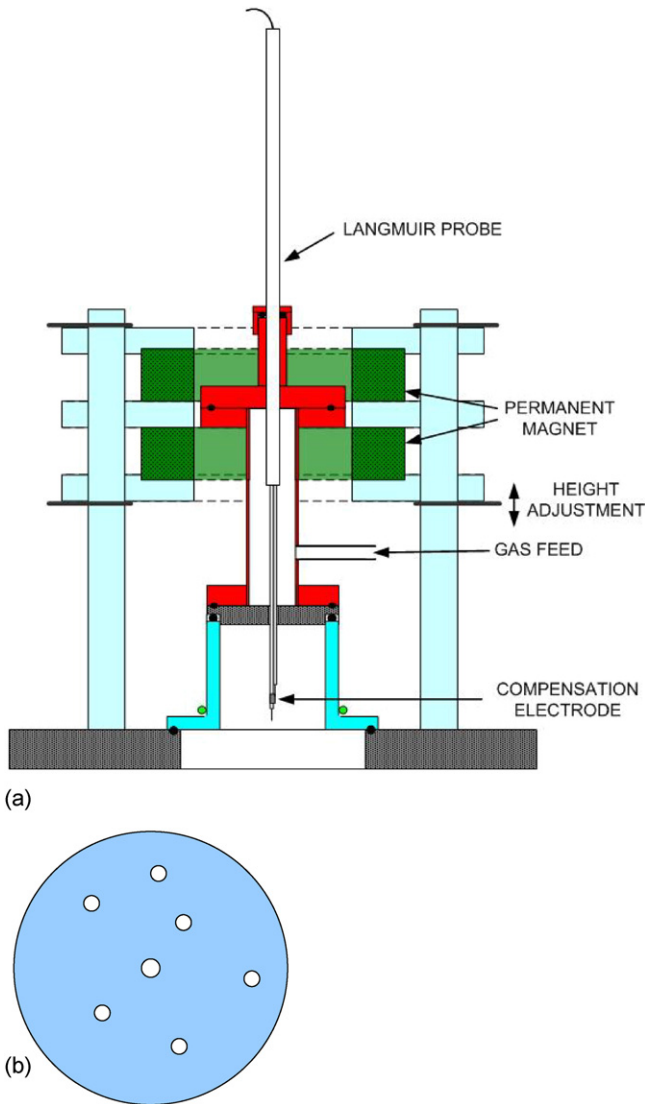


Figure 3. (a) Schematic of the helicon discharge with an extension chamber to accommodate the vertical probe. The dimensions are to scale. (b) Detail of the top plate with holes.

and the latter is spot-welded to a short 30 mil diameter tungsten rod in the large tube. A slip-joint then connects the current to the chokes. (A mil is 1/1000 inch, equal to 1/40 mm or 25 μm .) To use the OML theory, the probe radius should be as small as possible. Although we have used 3 mil diameter tips, they are too fragile for extended use. The tip diameter is nominal; it measures smaller with some micrometers, and it cannot be measured after exposure to ion bombardment for fear of breakage.

As shown by Sudit and Chen [19], inductors alone are insufficient for good RF compensation because of the stray capacitance and inductance of the wire connecting the lowest choke to the probe tip. An additional floating electrode (CE) needs to be added to drive the probe tip so that it follows the RF oscillations in plasma potential. Some commercial units include large CEs. Our CE is made of 1 mil Ni foil wrapped around the ceramic tube near the probe tip. The CE is approximately 1 cm long and is spot-welded to a 10 mil tungsten wire encased in another 1.6 mm diameter alumina

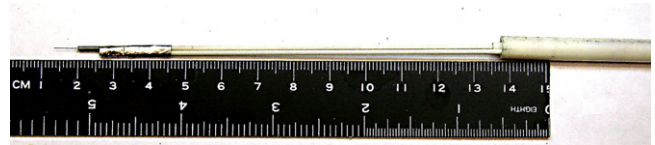


Figure 4. Photograph of the vertical probe with CE.

tube. Inside the larger shaft, this lead is connected the same way as the probe lead to a small capacitor soldered to the lowest choke. Both small tubes fit together through the 1/8 inch hole in the top plate. The hole also serves to center the probe. Figure 4 shows the probe with a 2 cm long CE. Since the CE must not touch the grounded top plate, measurements near the top cannot be made.

The choke chain is made to reject both 13.56 and 27.12 MHz oscillations. For high impedance Z at each frequency, the self-resonance frequency of hundreds of commercial chokes had been measured to choose models resonating at those frequencies. For 13 MHz, a single choke was found to have $Z \approx 1 \text{ M}\Omega$ in that vicinity, and particular samples of that model could have $Z \geq 400 \text{ k}\Omega$ at exactly 13.56 MHz. For 27 MHz, we found no choke with a peak near that frequency, but some models had $Z \geq 130 \text{ k}\Omega$ over a range beyond 27 MHz. Adding chokes in series increases the Z only slightly, and we found that the optimum was three 27 MHz chokes in series. However, the combination of one 13 MHz and three 27 MHz chokes had unexpected consequences. This is shown in the $Z(f)$ plots of figure 5. The 13 MHz choke alone measured almost 500 k Ω at 13.56. The three 27 MHz chokes alone gave $Z \approx 150 \text{ k}\Omega$. However, when they were connected together, the chokes interacted with one another, increasing $Z(27.12)$ to 300 k Ω while decreasing $Z(13.56)$ to 87 k Ω . Thus, the design of choke chains to suppress an RF frequency and its harmonics has to be done carefully.

2.3. Software

The electronic units for applying a sweeping voltage to the probe and measuring the current were supplied by Hiden Analytical, Ltd. Two systems were used. The older system, ESP Mk2, HAL IV, generates a linear sweep from -100 to $+100 \text{ V}$ or any range in between. The start and data dwell times are adjustable; that is, the delay between setting the voltage and measurement of current and the time during which the current is averaged at each step could be varied between 1 and 1000 ms. After testing, the shortest reliable dwells were set at 1 and 3 ms. The number of scans for each data point could be set, and the $I-V$ curves were recorded for each scan and for the average. The voltage trace for a two-scan data point is shown in figure 6(a). Each scan was from -100 to $+100 \text{ V}$, containing 500 points with dwells at 1 and 3 ms. It is seen that each scan takes about 5 s. The second system, ESPion[®], was designed for fast sweeps in pulsed plasmas and operated differently. Each 500-point sweep from -100 to $+100 \text{ V}$ takes only about 12 ms, as can be seen in figure 6(b), but the $I-V$ curve is extremely noisy. To overcome this, multiple scans can be taken and averaged by setting the quantity scan average (SA). Usable $I-V$ curves could be obtained with $\text{SA} = 4$, but

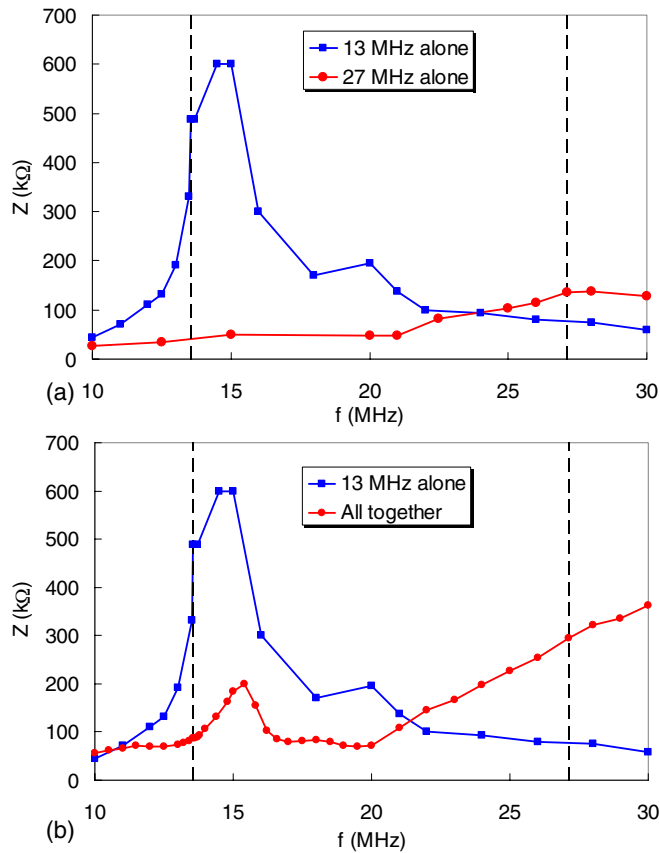


Figure 5. Impedance measurements of the choke chain (a) before and (b) after connecting the 13 and 27 MHz chokes together. The dashed lines mark the exact RF frequencies.

SA = 10–25 gave better curves. To obtain curves as smooth as with the ESP Mk2 required SA = 100. The speed of the ESPion system was needed in the very dense dc plasmas in this work in order to protect the probe. We also needed its maximum current of 1000 mA instead of 100 mA at our densities.

In both systems the current-measuring circuitry was on a floating circuit board which followed the probe voltage. Both systems had adjustments for the number of points in each scan. A probe cleaning voltage up to ± 100 V of adjustable duration could be applied before each scan in ESP Mk2 and before each bunch of scans in ESPion. However, since spurious voltages at high densities could harm the probe by ion sputtering or heating to electron emission, we cleaned the probe only once after each vacuum pumpdown.

3. Experiment

3.1. Effect of CE

Figure 7 shows the ion (I^2-V) and electron ($\ln I_e-V$) plots taken with a probe without a CE (chokes only). The ion plot (figure 7(a)) is almost exactly linear and is typical of all our data. The linearity is a characteristic of orbiting, but it also occurs incidentally in the ABR theory [20]. However, the ABR theory, which neglects orbiting, gives a spuriously low

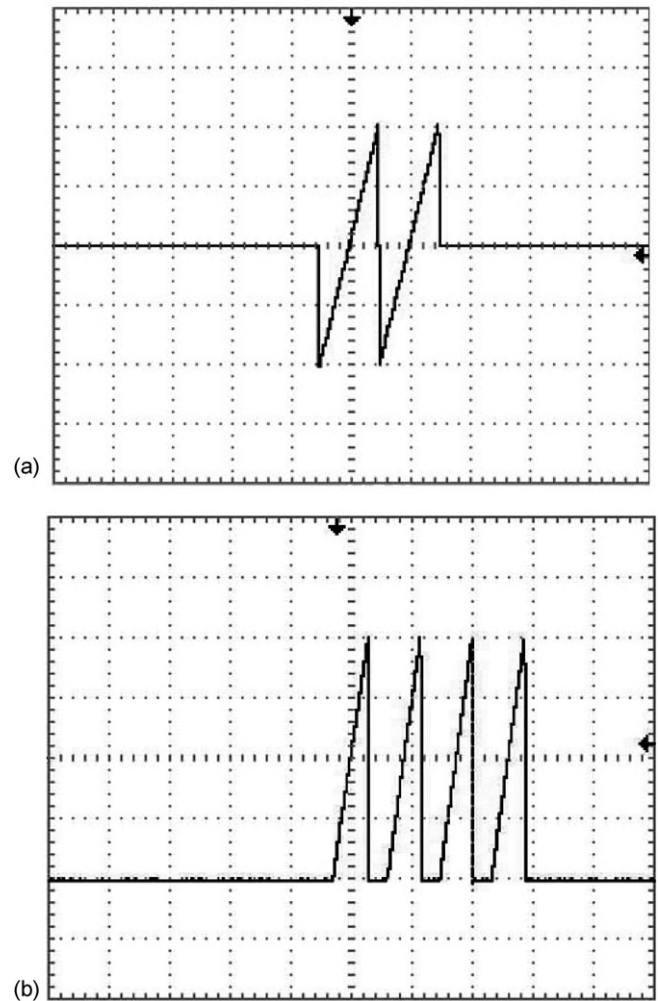


Figure 6. Voltage sweeps in the Hidden (a) ESP Mk2 and (b) ESPion probe systems. The vertical scale in both is 50 V/div, and the horizontal scales are (a) 5 s/div and (b) 25 ms/div.

density [10]. The density n_{11} in units of 10^{11} cm^{-3} (10^{17} m^{-3}) is obtained from equation (1) without the knowledge of T_e . The electron plots in figures 7(b) and (d) were obtained by subtracting the straight-line fit to the ion curve from the total current. We see that there are three regions showing three temperatures, as explained in figures 1 and 2. In figure 7(b), a fit to the slope at high V_p gives $KT_e = 4.65 \text{ eV}$, which is somewhat higher than the true temperature. In figure 7(c), a fit to the middle region, which is significantly affected by the RF, yields the spuriously high temperature of 8.22 eV. Such temperatures are often quoted as the true temperature when there is inadequate RF compensation. In figure 7(d), a fit to the left-most region gives the true temperature of 2.97 eV, since, as shown in figure 2, RF has little effect on I_i . Figure 7(e) shows a typical misinterpretation of T_e from a probe with too small a CE, and figure 7(f) shows the correct determination of T_e in the same plasma with a large enough CE. A large CE does not affect the spatial resolution of the probe tip, but it may affect the discharge if it is not small compared with the discharge volume.

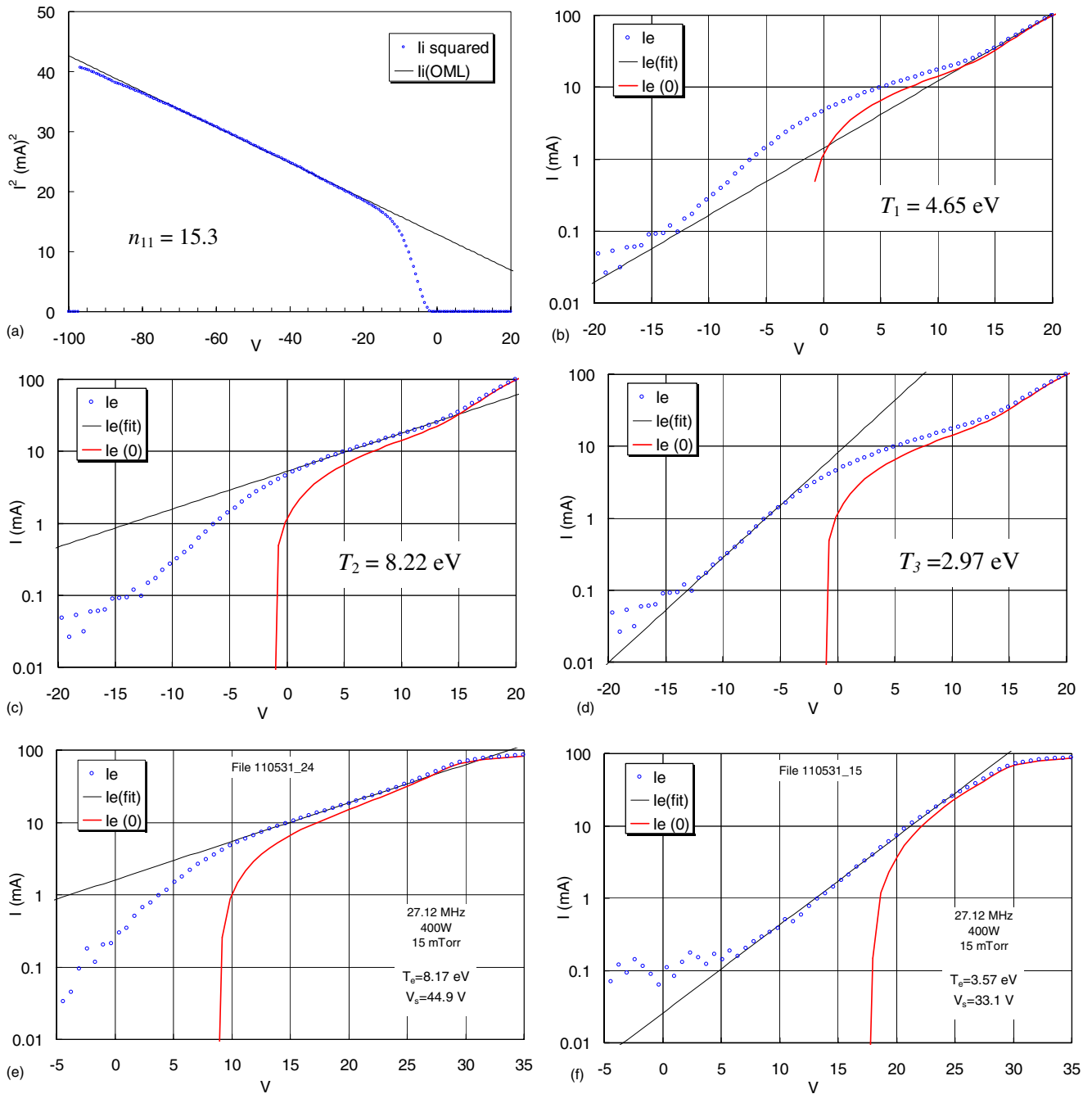


Figure 7. (a)–(d) I_i and I_e plots from a probe with no CE. Each region of the I_e plot is fitted to straight lines to give three different apparent values of T_e . The discharge was at high field: 280 G. (e)–(f) Example of (d) high T_e from a poorly compensated and (f) correct T_e from a well compensated probe in the same plasma.

3.2. Importance of ion subtraction

In the I_e plots, the solid red curve is the probe current before ion current is subtracted. The true T_e is best found from the region where the I – V curve is least affected by RF; namely, the region on the negative side of floating potential V_f . Hence, it is important to subtract the ion current from the total current accurately. This is a major finding in this work. Since our probe lies along the B -field, electrons can reach the probe only by cross-field diffusion. The saturation electron current is therefore smaller than normal, and the exponential part of the I_e curve is short. To obtain three e-foldings of I_e , we

have to use the part of $I_e(V_p)$ that is significantly affected by collection of ions.

3.3. RF amplitude

The amplitude of the RF oscillations in V_f (and presumably also in V_s) inside the discharge tube was measured with a floating probe connected directly to a digital scope. The signal everywhere was a pure sine wave at 27.12 MHz. The amplitudes are shown in figure 8. It is seen that the peak-to-peak amplitudes varied from about 12–50 V under the conditions of this experiment. This is about 4–12 times KT_e ,

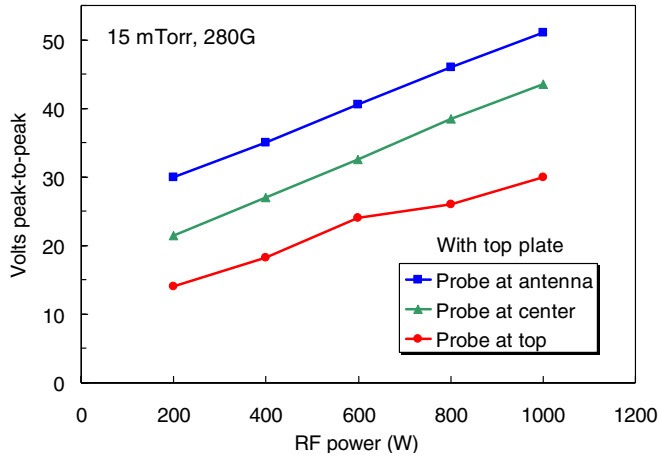


Figure 8. Peak-to-peak amplitude of RF oscillations in V_f versus P_{rf} at three positions in the discharge.

so that good RF compensation is essential. The B -field here was 280 G, much higher than the optimum field found later on.

3.4. Linear ion and electron curves

Since KT_e can be obtained from the ion-subtraction region of the electron characteristic, it is not necessary to record the entire $I-V$ curve. This will protect the probe from overheating at high electron currents. An ideal example of this procedure is given in figure 9, which was taken in the low-density plasma far below the source. The OML conditions are fulfilled, and the I^2-V curve is a perfectly straight line. The maximum current was limited to 1 mA, which was sufficient to give a straight line $\ln(I_e)$ plot to yield KT_e and V_s . The latter is given by the horizontal position of the straight-line fit in the $\ln(I_e)$ plot. The analysis was performed with an Excel file, not with the commercial software. We have analyzed hundreds of such curves, carefully finding the best straight-line fits to each. In almost all cases, the result shows a Maxwellian distribution of the high-energy electrons. It is reasonable to assume that if these electrons are Maxwellian, then the more collisional, low energy part of the distribution is also Maxwellian. We next discuss deviations from the ideal case of figure 9.

3.5. Impossibility of electron energy distribution function data

When the I^2-V curve is not straight, the $\ln(I_e)$ plot may also be curved in such a way as to suggest an ion or electron beam. An example is shown in figure 10. In (a) it is seen that the I^2-V curve is not completely straight, but no available theory (ABR, BRL or exact OML) could fit the curve. We could, however, fit a straight line to most of the curve. When this line was subtracted from the total current to yield I_e , a deviation from the linear $\ln(I_e)$ versus V_p fit shows an excess of high-energy electrons. Most commercial probe systems would use a highly filtered algorithm to obtain the electron energy distribution function (EEDF) from the second derivative of this curve. Such data cannot be trusted except in very well behaved plasmas. The excess electron current depends on how accurately the ion current was subtracted. The ion current should deviate

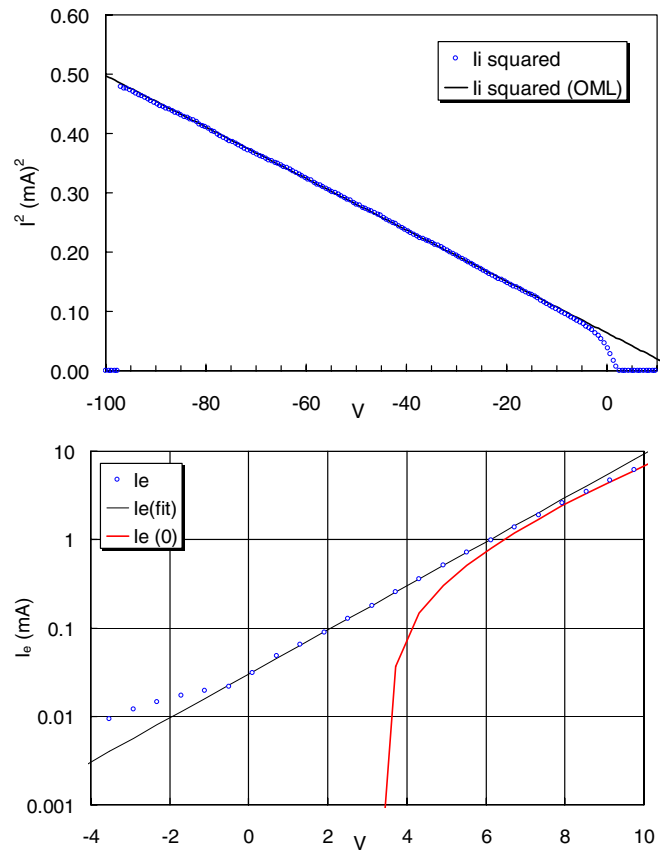


Figure 9. Ideal ion and electron curves downstream from the helicon source. Here $n = 0.8 \times 10^{11} \text{ cm}^{-3}$ and $KT_e = 1.6 \text{ eV}$.

from the straight line as V_p approaches V_f . If we fit a straight line to I_i^2 closer to V_f , as in (c), the resulting EEDF is a pure Maxwellian, as in (d). This is the best we can do, since we have no theory that predicts both the straight line at large $|V_p|$ and the curvature near V_f .

Godyak and Demidov [21] have shown beautiful non-Maxwellian EEDF curves in a laboratory RF plasma at lower densities and frequencies (and sometimes B -fields). We are unable to do this in a helicon plasma because the magnetic field prevents I_e from reaching its normal saturation. As pointed out by Bohm *et al* [22], electrons can reach the probe only by moving along the B -field, and I_e saturates at a current that depends on the rate of diffusion into the field lines that intersect the probe. This effect has been treated by numerous authors, including Bertotti [23] and Stangeby [24], and most recently by Popov *et al* [25]. Although it is possible, as we shall show later, to design RF compensation that gives the correct T_e up to the lowered I_e saturation current, our ion-subtraction technique gives the same result. It is not possible to verify theoretical EEDFs in the ion-subtraction region without extensive analysis of one case at a time.

3.6. Probe heating

We next consider the problem of probe heating in a dense plasma. Bombardment of the probe tip by ions or electrons deposits energy that can be lost by conduction or radiation.

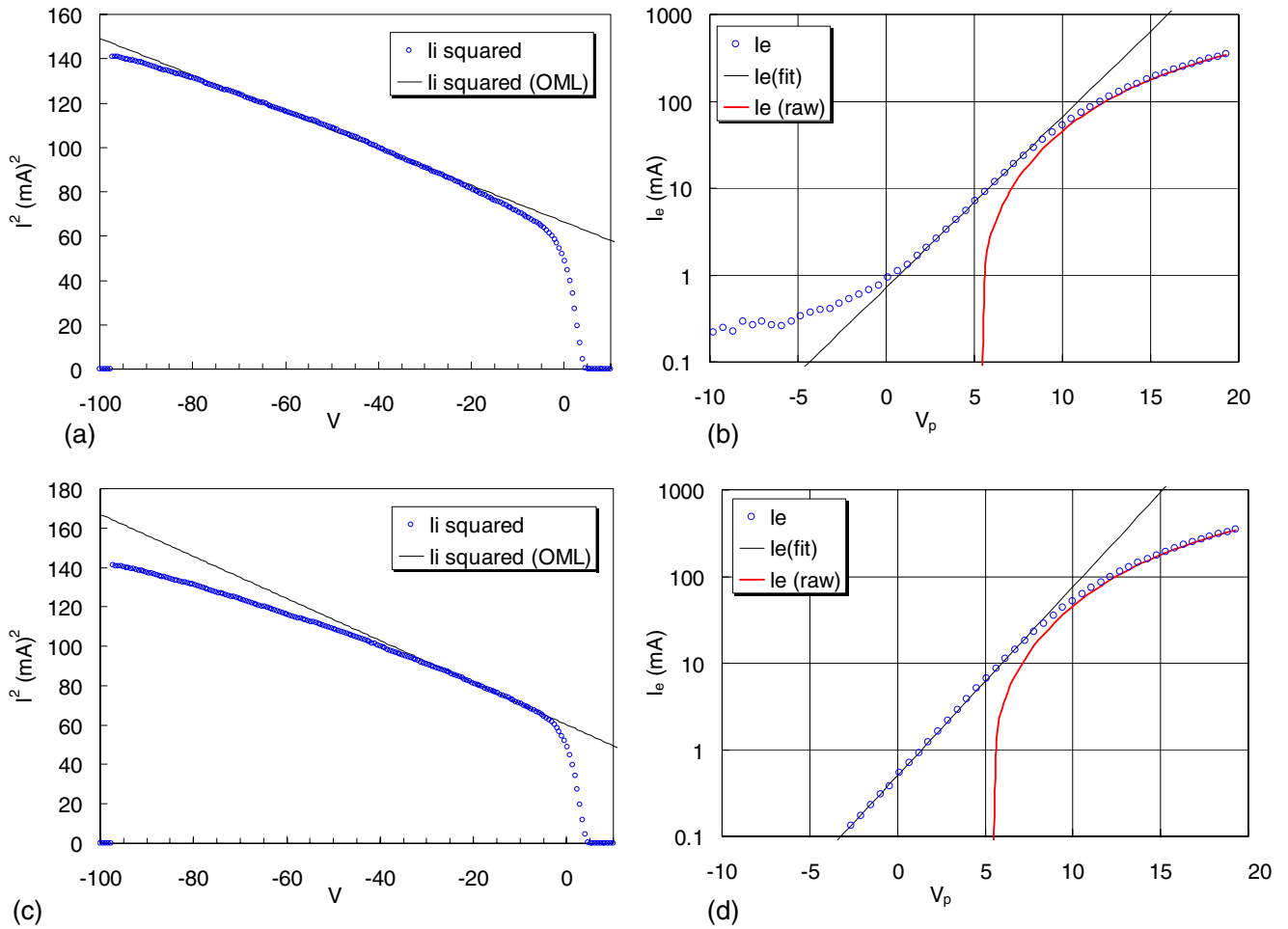


Figure 10. Example of an I - V curve that shows an electron tail that is not real. The data were taken with the ESPion software at the center of the discharge tube at 13.56 MHz, 400 W, 65 G, and 46 mTorr, and with scan average = 50. Analysis yields $n = 2.92 \times 10^{12} \text{ cm}^{-3}$, and $K T_e = 2.21 \text{ eV}$.

Since the probe is connected to a long, thin wire, conduction is negligible. The heat is lost by radiation according to the Stefan-Boltzmann law:

$$R = 5.68 \times 10^{-12} \varepsilon T^4 \text{ W cm}^{-2}, \quad (3)$$

where R is the radiated energy, ε is the emissivity of tungsten and T is the temperature in Kelvin. If V_p or the plasma comes in such short pulses that the probe tip does not come to a uniform temperature, its temperature will depend on the surface-to-volume ratio. In our case, the plasma runs steady state, and the probe tip is thin enough that it will be uniformly heated with normal scan times. From standard tables, R is shown in figure 11, together with electron emission, which occurs above about 2400 K. The slow sweep of the ESP Mk2 causes the probe to glow at high densities. An example in which this happens is shown in figure 12. The maximum I_i in this case was about 6 mA at -100 V , or about 15 W cm^{-2} . Assuming that the ESP Mk2 sweep is so slow that the probe comes to thermal equilibrium during the sweep, we find from equation (3) that the temperature corresponding to 15 W cm^{-2} during ion collection was about 1790 K. The maximum I_e at $V_p = +25 \text{ V}$ was about 100 mA, resulting in heating power of 62.7 W cm^{-2} . This radiation power yields a probe temperature

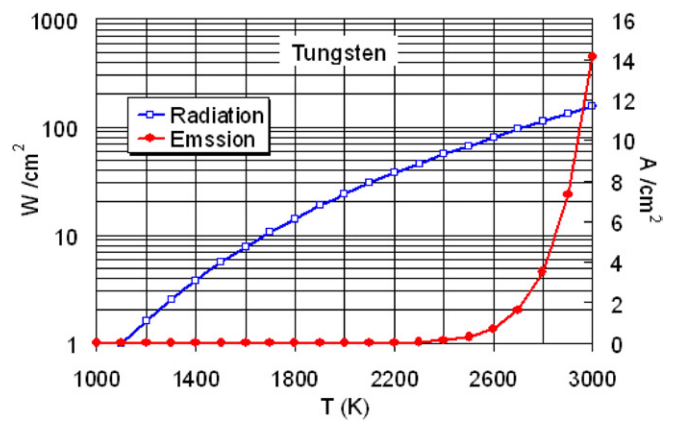


Figure 11. Optical radiation and electron emission from tungsten versus absolute temperature.

of 2550 K. This causes the probe to glow, but the probe glows even during ion collection if V_p is set for lower maximum electron current. Note that the probe area cancels out in this calculation. To avoid damaging the probe, we therefore operate well below electron saturation and are forced to obtain T_e from the ion-subtraction region. Fortunately, this gives the correct temperature.

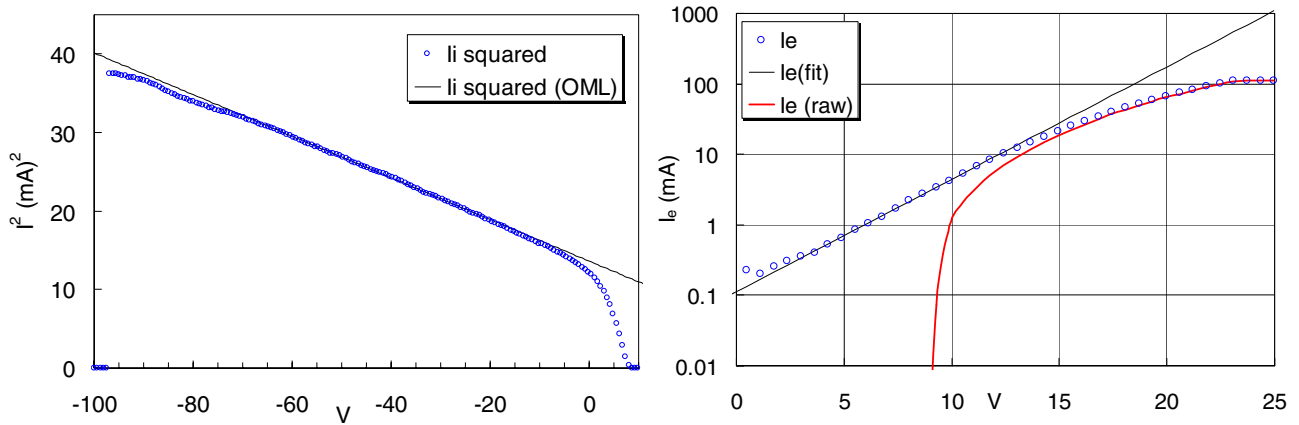


Figure 12. Ion and electron curves of a case when the probe glows. ESP Mk2 software, 13.56 MHz, 60 G, 400 W, 15 mTorr, $n = 1.65 \times 10^{12} \text{ cm}^{-3}$, $KT_e = 2.72 \text{ eV}$.

In some versions of the software, spurious square waves were found, typically -100 V for 1 s, not related to probe cleaning. These pulses would heat the probe unnecessarily, and it is advisable to check $V_p(t)$ before using the commercial software.

3.7. Operation with short scans

To collect higher electron current, we changed the software to ESPion, which takes the data in bunches of fast sweeps, as shown in figure 6(b). Remember that ESPion has a SA setting which set the number of scans in each bunch that are averaged. Without going into details, we have checked that the ESPion and ESP Mk2 systems give identical results in most cases, even though ESPion's ion curves are not as smooth if SA is less than about 50. This was instrumental: the discharge itself was checked to be completely free of low-frequency oscillations. The main difference in ESPion is in the 1000 mA current range setting, which is not available in the ESP Mk2. The 1000 mA range in ESPion gives correct currents at 13.56 MHz, but currents that are too high at 27 MHz. This is probably caused by the increased inductance of the 1Ω current-measuring resistor at 27 MHz, an effect which could exist in other systems as well. Note that the ion current at high $|V_p|$ dips below the straight line in figure 12. This is likely due to the formation of an absorption radius at high densities. At very low densities an opposite, upward curvature has been observed, which could be caused by large sheath expansion on a short probe, which then begins to act like a spherical probe.

3.8. Electron emission with scan bunches

Figure 13 shows the ESPion data of the same discharge as in figure 12, taken up to $V_p = +20 \text{ V}$ with SA = 10 and with the same 100 mA current range and 200 points per scan. The derived n and KT_e values are in reasonable agreement with those of figure 12. The probe does not glow. The pulse bunch is short enough that the probe tip does not come to thermal equilibrium and has enough heat capacity to absorb the particle energy without being heated to emit observable light.

If now the upper limit of the ESPion sweep voltage is raised, the probe will be first driven to a glowing temperature,

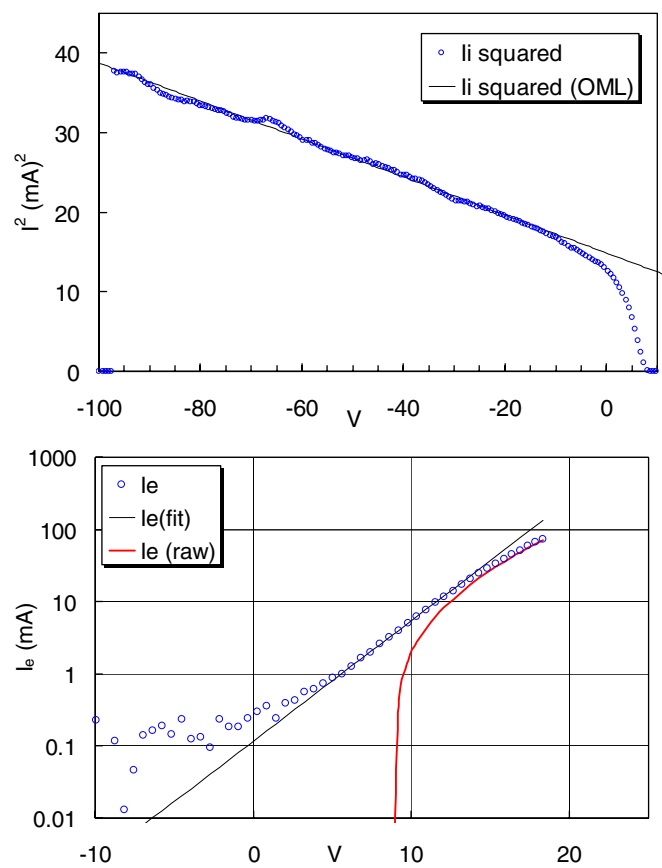


Figure 13. Ion and electron curves of the plasma of figure 12, but taken with the ESPion software. The derived n is $1.57 \times 10^{12} \text{ cm}^{-3}$ and $KT_e = 2.6 \text{ eV}$.

then start to emit electrons. Figure 14 shows that electron emission can also affect ion saturation current in scan bunches. The interaction occurs because the probe is heated by I_e during the first few scans of the bunch. On subsequent scans, I_i is measured while the probe is emitting electrons. In figure 14(a), a small amount of emission occurs as V_{max} (the maximum V_p in each scan) is raised from 15 to 50 V, with SA = 50. At $V_{\text{max}} = 50 \text{ V}$, n drops because SA was reduced to 25 to reduce the heating. At $V_{\text{max}} = 60$, n takes a big jump as

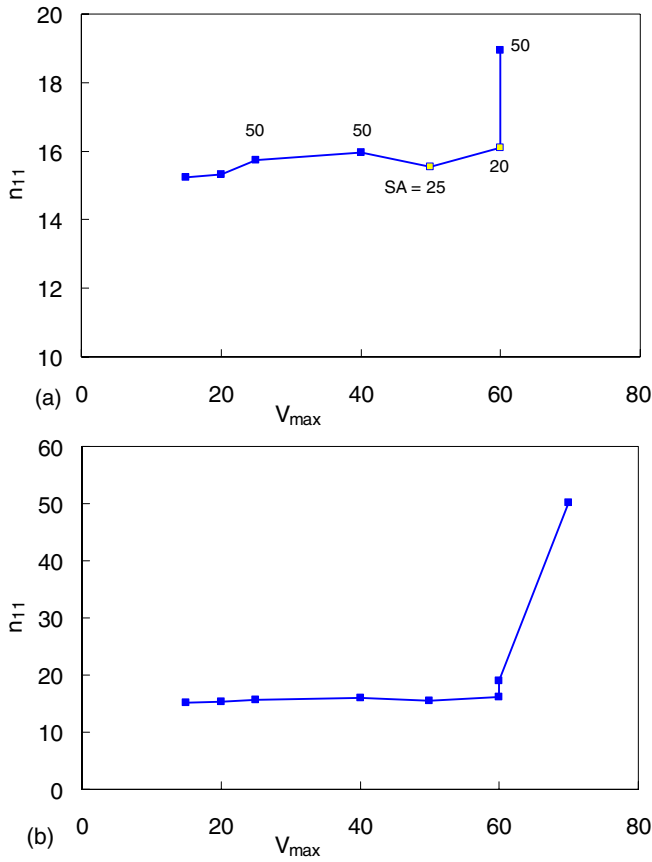


Figure 14. (a) Ion-derived densities versus maximum positive V_p on each scan using ESPion. (b) Same as (a) but extended to $V_{max} = 70$ V on a different scale. 400 W at 13.56 MHz, 65 G, 15 mTorr; probe at the center of discharge.

SA is increased back to 50. Figure 14(b) shows the same data on a smaller scale to show the $V_{max} = 70$ V point with $SA = 50$. The probe is in total emission, and n is significantly affected by electron emission. The $V_{max} = 70$ V I^2-V curve (not shown) looks exactly as that in figure 12 but with much higher values. The I_e curve for that case is shown in figure 15. At the $V_{max} = 70$ V point (actually 67 V), I_e was 46.8 mA. This corresponds to 786 W cm^{-2} and a probe temperature of 4800 K, according to equation (3). Clearly, the scans were fast enough that the probe did not reach thermal equilibrium.

3.9. Absence of transition region

In figure 15, electron saturation occurs at such low V_p that T_e could be obtained only from the ion-subtraction region, which extends nearly to I_e saturation. Setting V_{max} higher than 25 V is not necessary, since I_e is already saturated there. T_e can be measured without overheating the probe. This unusual situation is caused by the orientation of the probe along a strong B-field.

3.10. Design of CE

An attempt was made to improve RF compensation by making a larger CE. The sheath capacitance of the CE should be much larger than that of the probe tip. The sheath capacitance C_{sh}

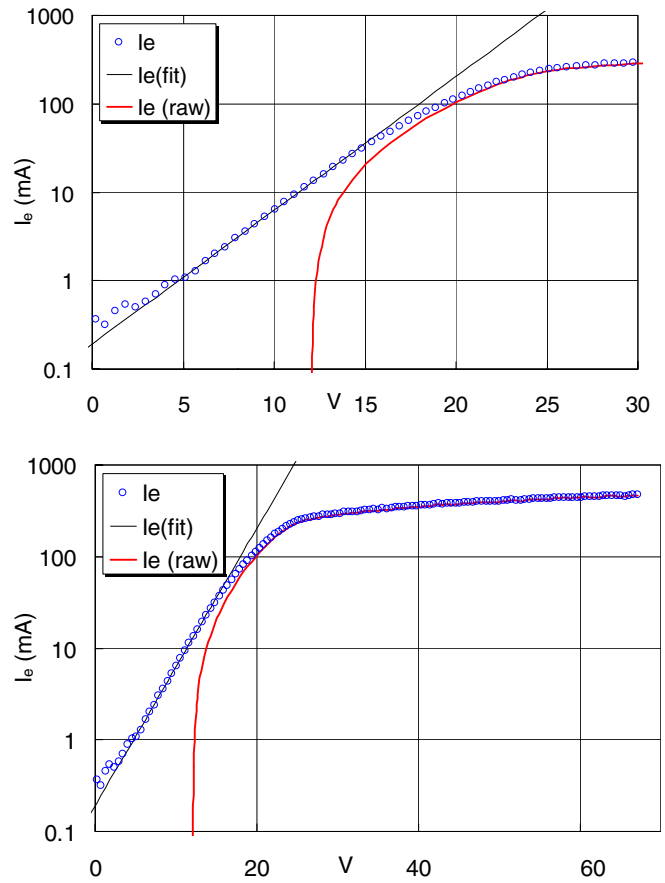


Figure 15. Electron curves for the $V_{max} = +70$ V case shown on two scales. At 2.87 eV, KT_e was normal.

has been calculated by many authors; for instance, by Godyak and Sternberg [26]. Using their method, Chen [27] gave C_{sh} as

$$\frac{C_{sh}}{A} = \frac{\epsilon_0}{\lambda_D} \frac{1}{\sqrt{2}} \frac{(1+2\eta)^{-1/2} - e^{-\eta}}{[(1+2\eta)^{1/2} + e^{-\eta} - 2]^{1/2}}, \quad (4)$$

where A is the probe area and η is the sheath drop normalized to KT_e . With A given by the area of the CE, the impedance of the sheath on the CE is given by $|Z_x| = 1/\omega C_{sh}$. This impedance then forms an RF voltage divider with the impedance $|Z_{ck}|$ of the choke chain. The requirement for the RF amplitude \tilde{V}_{rf} to be reduced to a small fraction of KT_e is then given by

$$\frac{e\tilde{V}_{rf}}{KT_e} \left| \frac{Z_x}{Z_{ck} + Z_x} \right| \approx \frac{e\tilde{V}_{rf}}{KT_e} \left| \frac{Z_x}{Z_{ck}} \right| \ll 1. \quad (5)$$

Using the value of \tilde{V}_{rf} from figure 8 and that of $|Z_{ck}|$ from figure 5, we then determined that our CE should be 2 cm long instead of 1 cm. Such a CE was made and inserted, but it could not be withdrawn into the 1/8 inch hole without touching ground and was so large compared with the small discharge that no good data could be taken with it. In this exercise we also tried leaving the connecting wire of a 1.2 cm long CE unshielded, thus requiring only one thin alumina tube to be inserted into the discharge. This made no difference, and figure 15, for instance, was taken with such a bare wire.

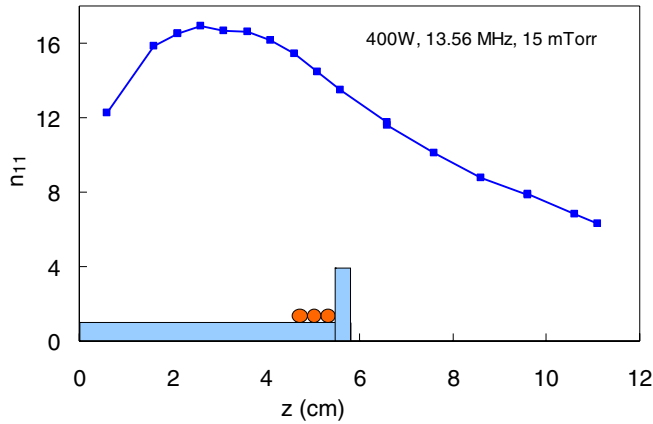


Figure 16. Axial density profile in units of 10^{11} cm^{-3} in a 13.56 MHz helicon discharge at 400 W, 15 mTorr of Ar, and a 65 G average B -field.

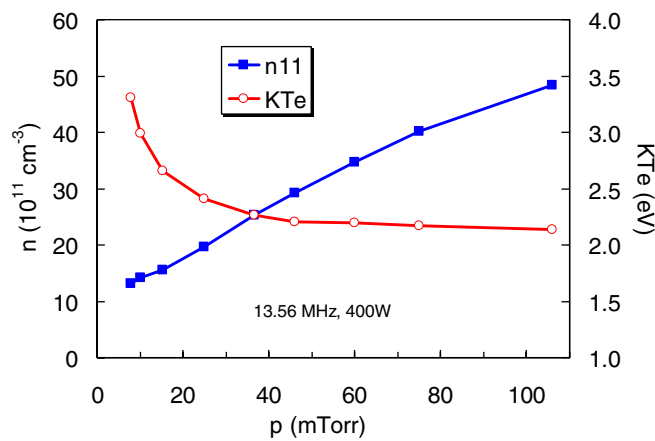


Figure 17. Pressure scan of n and KT_e at the center of the plasma.

3.11. Examples of data

Here we give examples of data taken of the discharge inside the tube using the techniques described above. The axial profile of density is shown in figure 16 in relation to the tube. The CE was 1.2 cm long, connected to the probe with a bare wire. The farthest point reached by the vertical probe is only a few mm above a horizontal probe with a very large CE. The densities measured with the two probes were in absolute agreement. Figure 17 shows the pressure dependence of density at the center of the discharge under the same conditions. The electron temperature falls with increasing pressure in agreement with theory.

Figure 18 shows a power scan from 200 to 1000 W into the antenna. The probe is located at the center of the discharge. Surprisingly, the density is not proportional to the power, as it is downstream in the chamber into which the plasma is ejected, as shown in figure 19. The maximum densities observed inside the tube are less than $5 \times 10^{12} \text{ cm}^{-3}$, whereas densities in a long cylinder would be an order of magnitude higher. This is because the plasma created does not stay long inside the tube and therefore does not build up normally there. The ‘saturation’ of the curve in figure 18 may indicate a faster ejection of plasma at higher RF powers. The physics of the

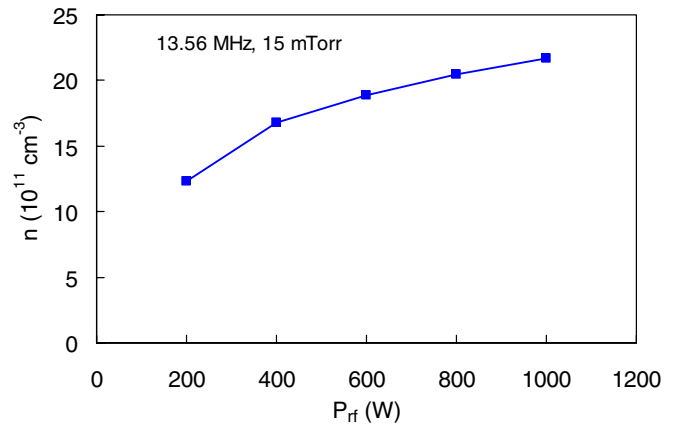


Figure 18. Power scan with the vertical probe inside the discharge at 13.56 MHz, 65 G, and 15 mTorr.

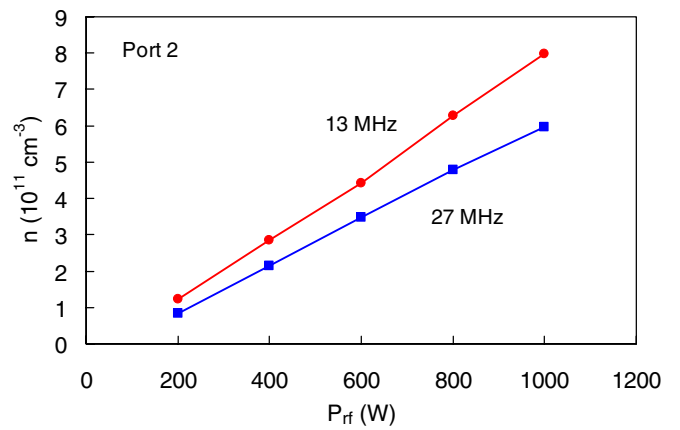


Figure 19. Power scans at 132 and 27 MHz with a horizontal probe 16.9 cm below the discharge.

discharge will be discussed in a separate paper not limited to diagnostics.

4. Summary

- (1) Langmuir probe measurements inside the intense RF environment of a magnetized (helicon) discharge were made successfully.
- (2) The ion I^2-V plots are closely linear even at densities well beyond the validity of the OML theory. The dependence of I_i on $V_p^{1/2}$ stems from conservation of energy and angular momentum of monoenergetic ions impinging on a cylindrical probe. However, the OML formula which does not contain T_i can only be derived from Langmuir’s theory for a Maxwellian ion distribution in the limit $T_i \rightarrow 0$.
- (3) The effect of the magnetic field and collisions on electron current not only ‘round off’ the knee of the $\ln(I_e) - V_p$ curve but can reduce electron current to such an extent that the linear Maxwellian region is absent altogether.
- (4) Electron temperature, however, can be obtained correctly by subtracting the linear fit to the ion I^2-V curve to extract the electron current from the total current. Using the ‘ion-subtraction region’ avoids incorrect high T_e s seen with insufficient RF compensation.

- (5) It is not possible to measure the electron distribution function, since the available region of probe voltages contains ion current, which must be subtracted approximately by linear extrapolation.
- (6) The RF amplitude inside the discharge was measured, and its relation to the required size of the compensation electrode is shown.
- (7) The effect of long and short scan times on probe heating is demonstrated, and heating up to electron emission is observed.
- (8) Self-resonant inductors for RF filtering cannot simply be connected together in series because they interact with one another.

References

- [1] Klagge S and Maass M 1983 *Beitr. Plasmaphys.* **23** 355
- [2] Hershkowitz N 1989 How Langmuir probes work *Plasma Diagnostics* vol 1, ed O Auciello and D L Flamm (San Diego, CA: Academic) p 169
- [3] Lieberman M A and Lichtenberg A J 2005 *Principles of Plasma Discharges and Materials Processing* 2nd edn (Hoboken, NJ: Wiley-Interscience) p 202
- [4] Mott-Smith H M and Langmuir I 1926 *Phys. Rev.* **28** 727
- [5] Allen J E, Boyd R L F and Reynolds P 1957 *Proc. Phys. Soc. (London)* B **70** 297
- [6] Bernstein I B and Rabinowitz I N 1959 *Phys. Fluids* **2** 112
- [7] Laframboise J G 1966 University of Toronto Institute for Aerospace Studies Report No 100, unpublished
- [8] Chen F F 1965 *J. Nucl. Energy Pt. C* **7** 47
- [9] Chen F F 2001 *Phys. Plasmas* **8** 3029
- [10] Chen F F, Evans J D and Zawalski W 2012 Calibration of Langmuir probes against microwaves and plasma oscillation probes *Plasma Sources Sci. Technol.* **21** 055002
- [11] Chen F F 2009 *Plasma Sources Sci. Technol.* **18** 035012
- [12] <http://www.hiddenanalytical.com/index.php/en/product-catalog/51-plasma-characterisation/80-hidden-espion-advanced-langmuir-probe-for-plasma-diagnostics>
- [13] www.impedans.com
- [14] <http://www.pnasol.com>
- [15] Chen F F and Torreblanca H 2007 *Plasma Phys. Control. Fusion* **49** A81
- [16] Chen F F and Torreblanca H 2009 *Phys. Plasmas* **16** 057102
- [17] Chen F F and Torreblanca H 2011 *IEEE Trans. Plasma Sci.* **39** 2452
- [18] Chen F F 2003 *Phys. Plasmas* **10** 2586
- [19] Sudit I D and Chen F F 1994 *Plasma Sources Sci. Technol.* **3** 162
- [20] Chen F F 1965 *J. Appl. Phys.* **36** 675
- [21] Godyak V A and Demidov V I 2011 *J. Phys. D: Appl. Phys.* **44** 233001
- [22] Bohm D, Burhop E H S and Massey H S W 1949 *Characteristics of Electrical Discharges in Magnetic Fields* ed A Guthrie and R K Wakerling (New York: McGraw-Hill)
- [23] Bertotti B 1961 *Phys. Fluids* **4** 1047
- [24] Stangeby P C 1982 *J. Phys. D: Appl. Phys.* **15** 1007
- [25] Popov Tsv K, Ivanova P, Dimitrova M, Kovacic J, Gyergyek T and Cercek M 2012 *Plasma Sources Sci. Technol.* **21** 025004
- [26] Godyak V A and Sternberg N 1991 *Proc. 20th Int. Conf. on Phenomena in Ionized Gases (Barga, Italy)* p 661
- [27] Chen F F 2006 *Plasma Sources Sci. Technol.* **15** 773